

Accepted Manuscript

Title: A spectrophotometer-based diffusivity assay reveals that diffusion hindrance of small molecules in extracellular matrix gels used in 3D cultures is dominated by viscous effects

Author: Roland Galgoczy Isabel Pastor Adai Colom Alicia Giménez Francesc Mas Jordi Alcaraz



PII: S0927-7765(14)00252-5
DOI: <http://dx.doi.org/doi:10.1016/j.colsurfb.2014.05.017>
Reference: COLSUB 6422

To appear in: *Colloids and Surfaces B: Biointerfaces*

Received date: 13-3-2014
Revised date: 2-5-2014
Accepted date: 9-5-2014

Please cite this article as: R. Galgoczy, I. Pastor, A. Colom, A. Giménez, F. Mas, J. Alcaraz, A spectrophotometer-based diffusivity assay reveals that diffusion hindrance of small molecules in extracellular matrix gels used in 3D cultures is dominated by viscous effects, *Colloids and Surfaces B: Biointerfaces* (2014), <http://dx.doi.org/10.1016/j.colsurfb.2014.05.017>

This is a PDF file of an unedited manuscript that has been accepted for publication. As a service to our customers we are providing this early version of the manuscript. The manuscript will undergo copyediting, typesetting, and review of the resulting proof before it is published in its final form. Please note that during the production process errors may be discovered which could affect the content, and all legal disclaimers that apply to the journal pertain.

A spectrophotometer-based diffusivity assay reveals that diffusion hindrance of small molecules in extracellular matrix gels used in 3D cultures is dominated by viscous effects

Roland Galgoczy^a, Isabel Pastor^b, Adai Colom^{a,1}, Alicia Giménez^a, Francesc Mas^b, Jordi Alcaraz^{a,c,*}

^a Unitat de Biofísica i Bioenginyeria, Facultat de Medicina, Universitat de Barcelona, Barcelona 08036, Spain

^b Departament de Química-Física, Institut de Recerca de Química Teòrica i Computacional (IQTUB), Universitat de Barcelona, Barcelona 08028, Spain

^c CIBER de Enfermedades Respiratorias, Bunyola 07110, Spain

¹ Present address: U1006 INSERM, Université Aix-Marseille, 13009 Marseille, France

*Corresponding author:

Jordi Alcaraz

Unitat de Biofísica i Bioenginyeria, Facultat de Medicina, Universitat de Barcelona

Casanova 143, 08036 Barcelona, Spain

Tel: (+34) 93 402 4515; Fax: (+34) 93 403 5278

e-mail: jalcaraz@ub.edu

Keywords: diffusion, Matrigel, collagen, fibrin, 3D culture, Stokes-Einstein equation

Word count: 6219 (including references)

Abstract

The design of 3D culture studies remains challenging due to the limited understanding of extracellular matrix (ECM)-dependent hindered diffusion and the lack of simple diffusivity assays. To address these limitations, we set up a cost-effective diffusivity assay based on a Transwell plate and the spectrophotometer of a Microplate Reader, which are readily accessible to cell biology groups. The spectrophotometer-based assay was used to assess the apparent diffusivity D of FITC-dextrans with molecular weight (4-70 kDa) spanning the physiological range of signaling factors in a panel of acellular ECM gels including Matrigel, fibrin and type I collagen. Despite their technical differences, D data exhibited ~15% relative difference with respect to FRAP measurements. Our results revealed that diffusion hindrance of small particles is controlled by the enhanced viscosity of the ECM gel in conformance with the Stokes-Einstein equation rather than by geometrical factors. Moreover, we provided a strong rationale that the enhanced ECM viscosity is largely contributed to by unassembled ECM macromolecules. We also reported that gels with the lowest D exhibited diffusion hindrance closest to the large physiologic hindrance of brain tissue, which has a typical pore size much smaller than ECM gels. Conversely, sparse gels (≤ 1 mg/ml), which are extensively used in 3D cultures, failed to reproduce the hindered diffusion of tissues, thereby supporting that dense (but not sparse) ECM gels are suitable tissue surrogates in terms of macromolecular transport. Finally, the consequences of reduced diffusivity in terms of optimizing the design of 3D culture experiments were addressed in detail.

1. Introduction

All tissue cells are attached to an extracellular matrix (ECM), which provides the physiologic fibrillar scaffold required for tissue organization. In addition to mechanical support, ECM provides biochemical cues that are critical regulators of cellular fate. The recognition of the important ECM regulatory role *in vivo* has extended the use of three-dimensional (3D) cultures based on growing cells embedded in gels of native ECM components [1, 2]. Thus, the availability of ECM macromolecules from major tissue types including type I collagen (COL1) and reconstituted basement membrane (rBM, also known as Matrigel or EHS matrix) has enabled using 3D cultures to study different cell types in a variety of physiopathological processes such as differentiation, morphogenesis and invasion [3-6].

A major role of ECM *in vivo* is to hinder the diffusion of soluble signaling factors [7, 8]. Likewise, diffusion hindrance has also been reported in ECM gels used in 3D cultures [5, 9], although the extent to which gels mimic tissue hindrance is not well established. In addition to the ECM, hindered diffusion in 3D cultures is contributed by cells. The latter contribution has been analyzed both experimentally and theoretically, and has been largely attributed to the geometrical obstacles posed by cells [8, 10, 11]. Likewise, the diffusivity of macromolecules in free solution and agarose gels have been extensively studied [7, 12, 13]. In contrast, quantitative analyses of their diffusivity in ECM gels are still scarce, and the physical basis underlying ECM-dependent hindrance in conditions relevant for 3D cultures remains overall ill defined [8, 10].

In addition to ECM-dependent effects, reduced diffusion depends on the physicochemical properties of the diffusing particle and on ECM-particle interactions [8, 14]. A major consequence of these multi-factorial effects is that the design and interpretation of 3D culture

experiments require detailed knowledge of the diffusivity of the target signaling factor(s) within the specific ECM gel. Common approaches to assess diffusivity in gels include fluorescence recovery after photobleaching (FRAP) and fluorescence correlation spectroscopy (FCS). However, the latter microscopic approaches are challenging for most cell biology groups working with 3D cultures, since they require access to expensive instrumentation including a confocal microscope, expert personnel and advanced numerical analysis tools. Alternatively, a less challenging approach has been reported in chemotaxis assays in which diffusivity of fluorescently labelled tracers is assessed by time-lapse fluorescence intensity measurements by fluorescence microscopy. However, these chemotaxis assays are still limited in that they require customized sample holders [15, 16].

To overcome the above limitations, we sought to set-up and validate a simple and cost-effective diffusivity assay based on a sample holder (i.e. Transwell plates) and a fluorescence recording device (i.e. spectrophotometer in a Microplate Reader) that are easily available in most cell biology laboratories. Next, we used the spectrophotometer-based assay to assess the diffusivity of tracer particles (FITC-conjugated dextrans) with molecular weights (M_r) spanning the physiological range of signaling factors in a panel of ECM gels as used in 3D cultures [17]. Diffusivity data were analyzed to unravel the role of gel density, geometry and viscous friction in controlling diffusion hindrance. In addition, guidelines to improve the design of 3D cultures in terms of transport were provided.

2. Material and methods

2.1. ECM gels

Gels were prepared at densities known to elicit physiologic responses in 3D culture studies [3, 5, 6]. rBM solution was used undiluted (12 mg/ml, Cultrex BME, Trevigen). COLI solution was prepared in serum-free culture medium (SFM) as reported elsewhere [2] to a final density of either 1 or 3 mg/ml, which were referred to as sparse (1) and dense (3) densities owing to the proteolytic-independent and dependent cellular invasion observed in these gels, respectively [6]. Dense fibrin (FIB) was prepared as previously described [2]. For spectrophotometer-based diffusivity experiments, each gel sample and experimental condition was prepared in triplicates in Transwell plates (24 Transwell plate, 8 μ m pore size, 6.5 mm wide insert, Corning) that contained two separate units: the top Transwell insert and the bottom lower Transwell compartment (Fig. 1A). The day of the experiments, 70 μ l of either rBM or COLI solution were added to the bottom of a Transwell insert, loaded into the lower Transwell compartment, kept in an incubator (37°C, 95% humidity) for 30 min to enable gelation, and hydrated with 200 μ l SFM. For FIB gels, 70 μ l of fibrinogen+thrombin solution were added to the Transwell insert, kept at room temperature for 5 min, incubated at 37°C and hydrated with SFM. The theoretical gel thicknesses were 2 mm, which is commonly used in 3D cultures [17, 18]. For FRAP experiments, 70 μ l of each ECM solution were polymerized onto an 8-chamber culture slide (BD Falcon).

2.2. Spectrophotometer-based diffusivity measurements

The diffusion of FITC-dextran at 3 different M_r (4, 40 and 70 kDa, referred to as Dex4, Dex40 and Dex70 thereafter) (Sigma) through gel samples prepared in Transwell Plates was

monitored with a Microplate Reader as described in Fig. 1A. Each condition was examined with a three-step protocol. First, the SFM on top of each Transwell insert was removed and replaced with 200 μl of 1 mg/ml dextran solution prepared in SFM. Second, each insert was loaded into a lower Transwell compartment containing 1000 μl SFM. Transwells without gels were used as negative controls. Third, the dextrans that had diffused throughout the gel to the lower Transwell compartment were monitored as a function of time by measuring the total fluorescence intensity in the lower compartment (F_{PR}) with a Microplate Reader (Synergy 2 Multi-Mode Microplate Reader, BioTek) in fluorescence mode, using wavelength excitation and emission filters of 485/20 nm and 528/20 nm, respectively. For this purpose, inserts were quickly removed and transferred to an adjacent empty well before F_{PR} readings, and put back into their original compartments to continue accumulating dextrans. F_{PR} was read at time intervals of 5 min during the first hour, and of 1 h up to 8 h. Preliminary studies indicated that measuring F_{PR} of each experimental condition required ~ 30 s, which was short enough to not compromise the expected slow monotonic increase of F_{PR} with time, even in the fastest diffusivity conditions. For each time point, F_{PR} was averaged for all repeated measurements ($n=3$). Transwells were kept in an incubator between measurements to minimize water evaporation.

To model our spectrophotometer-based diffusion measurements, we used a common approach based on considering hydrogels as a porous medium. In these conditions, the one-dimensional (1D) Fick's law of diffusion applies

$$\frac{\partial c}{\partial t} = D \frac{\partial^2 c}{\partial x^2} \quad (1)$$

where $C(x,t)$ is the concentration of diffusing particles as a function of time (t) and depth (x), and D is the isotropic diffusion coefficient inside the gel. The simplest and most widely used strategy to solve Eq. (1) for the diffusion of an extended initial particle distribution C_0 assumes that the hydrogel is a semi-infinite slab, which corresponds to $C(x \geq 0, t = 0) = 0$, $C(x \rightarrow \infty, t \geq 0) = 0$, and $C(x = 0, t \geq 0) = C_0$ [5, 11, 15], thereby eliciting [19]

$$C(x, t) = C_0 \cdot \operatorname{erfc} \frac{x}{2\sqrt{Dt}} \quad (2)$$

where erfc is the error function complement. Eq. (2) is a suitable approximation to model the diffusion within a finite-sized material when the thickness of the diffusion layer δ during the experimental time-window is smaller than that of the material, where δ can be assessed as [15, 20].

$$\delta = \sqrt{2Dt} \quad (3)$$

We adapted Eq. (2) to model our measurements as

$$C_l(t) = C_0 \cdot \operatorname{erfc} \frac{l}{2\sqrt{Dt}} \quad (4)$$

where l is the gel depth and $C_l(t)$ is the dextran concentration at $x = l$. Eq. (4) was fitted to the average F_{PR} data by nonlinear least-squares fitting (MATLAB, The Mathworks), being l and the apparent diffusivity D fitting parameters. As initial fitting values we used $l = 2$ mm and D

predicted by the Stokes-Einstein (S-E) equation for water [7]. For each experimental condition, the time window used to fit Eq. (4) was taken up to 50% of the last F_{PR} data point to guarantee $\delta < l$. Eq. (4) was also used to assess the time to reach 50% of C_0 (t_{50}) by imposing $\text{erfc } 0.5l/(Dt)^{1/2} = 0.5$ using MATLAB, which elicited

$$t_{50} = \frac{l^2}{0.9D} \quad (5)$$

The effective viscosity η was assessed from D data using the S-E equation [7]

$$\eta = \frac{k_B T}{6\pi D R_H} = \frac{k_B T}{6\pi D} \left(\frac{4\pi\rho}{3M_r} \right)^{\frac{1}{3}} \quad (6)$$

where k_B is the Boltzmann's constant, T is the absolute temperature, ρ is the particle's density and R_H is the hydrodynamic radius. The latter was assessed using an empirical relation [21] that elicited 1.21 nm for Dex4, 4.12 nm for Dex40 and 5.55 nm for Dex70.

2.3. Diffusivity measurements by FRAP

Dex4 solution was added to each ECM gel 3 days before experiments to enable reaching near-equilibrium concentrations [5] and kept at 37°C. FRAP measurements were conducted with a scanning confocal microscope (TCS SP2 UV, Leica). Samples were illuminated with a 10× 0.4 NA objective and a 488 nm excitation line from a 30 mW Ar⁺ laser operating at 8% output power. Photobleaching of a 40 μm wide circular region-of-interest (ROI) was achieved with a

488 and 514 nm excitation line from the Ar⁺ laser at 100% of relative intensity. The bleaching time was 1.4 s, and the total ROI fluorescence intensity images after photobleaching were collected at intervals of 0.28 ms up to 50 s at 512×512 pixel resolution using a pinhole of 1 Airy unit (n=6 per gel type). These settings minimized the fluorescence contribution from the diffusion of FITC-dextran along the axial direction and prevented any recovery during bleaching [22]. FRAP measurements were modeled assuming that the bleached area had a uniform circular disk profile, which enabled analyzing all the recovery curves with [23]:

$$F_{ROI}(t) = [F_{\infty} - F_0] \left[\exp\left(-\frac{2\tau_D}{t}\right) \left[I_0\left(\frac{2\tau_D}{t}\right) + I_1\left(\frac{2\tau_D}{t}\right) \right] \right] + F_0 \quad (7)$$

where $F_{ROI}(t)$ is the normalized mean fluorescence intensity in the bleached ROI at t , F_{∞} is the recovered fluorescence at large t , F_0 is the bleached fluorescence intensity right after the bleach, τ_D is a characteristic residence time of the diffusing particle in a volume of characteristic length ω , and I_0 and I_1 are the modified Bessel Functions. Eq. (7) was nonlinear least-squares fitted to FRAP measurements with MATLAB, being τ_D a fitting parameter, which was used to assess the effective diffusion coefficient as $D_{FRAP} = \omega^2/4\tau_D$. D_{FRAP} data were averaged for all repeated measurements (n=6).

2.4. AFM imaging

To enhance AFM resolution, gels were prepared as in 2.1. and fixed with 1% glutaraldehyde (Sigma) PBS solution for 30 min to render stiffer gels [24]. Samples were imaged

in PBS at room temperature with a commercial AFM (Bioscope I, Veeco) by raster scanning a V-shaped cantilever (0.01 nN/nm, 20 nm tip radius, MLCT, Veeco) over a scan size of 20-40 μm at low scan rate (≤ 0.2 Hz) in contact mode, using a minimum feedback loading force. Images were obtained in different locations (≥ 5) of each gel ($n=2$), and flattened with WSxM software [25]. For each image, pore edges were outlined manually and their corresponding areas were assessed with IMAGE J [26]. The pore width (w) for each pore area (A) was calculated as $w = 2(A/\pi)^{1/2}$.

2.5. Statistical analysis

Differences were examined by either Student's t -test or Mann-Whitney test for not normally distributed populations (SigmaPlot, Systat Software). Statistical significance was assumed at $P < 0.05$. Unless otherwise stated, data are given as mean \pm SE.

3. Results

3.1. Validation of the spectrophotometer-based diffusivity assay

A scheme of the spectrophotometer-based diffusivity assay is shown in Fig. 1A. The maximum gel dextran equilibrium concentration was ~ 150 $\mu\text{g}/\text{ml}$, which fell within the linear detection regime of the Microplate Reader as shown in Fig. 1B. The average F_{PR} data corresponding to the diffusion of Dex4 in all conditions are shown in Fig. 1C, where F_{PR} were normalized to the maximum fluorescence recorded in SFM. A monotonic increase of normalized F_{PR} with time was observed even in the fastest diffusivity conditions of Dex4 in sparse COLI, thereby supporting the feasibility of our approach in ECM gels. In SFM, F_{PR} exhibited a modest

and slow decline at longer times after reaching its maximum at ~ 1 -2h. A similar drop in F_{PR} was observed in wells with a constant dextran concentration of 150 $\mu\text{g/ml}$ examined at the same time points as in Fig. 1C (data not shown), supporting that it was associated with photobleaching. For subsequent analysis, only F_{PR} data up to 50% of their final value were used to guarantee $\delta < l$ according to Eq. (3). The corresponding fittings obtained with Eq. (4) are shown in Fig. 1C (continuous lines). By restricting the analysis of F_{PR} data within the diffusion layer, the time window used in the fittings in SFM was ~ 5 min. In these conditions, the drop in F_{PR} due to photobleaching was negligible ($< 2\%$), supporting further the feasibility of our data analysis. As a guidance, we also included the fittings of the semi-infinite model over the entire data range (dotted lines). The model captured accurately the dynamics of the intensity data in both time-windows ($r^2 \geq 0.95$). Similar results were obtained with the other dextrans (Suppl. Fig. S1). Likewise, fitted l values were very close to the theoretical 2 mm in all conditions examined (data not shown).

D data obtained from the fittings are summarized in Table 1 and Suppl. Table S1, and were first validated by comparing D assessed in SFM (D_{SFM}) with the corresponding theoretical values computed with the S-E equation (D_o) taking the water viscosity at 37°C (0.69 mPa·s) [27]. Both D_{SFM} and D_o values exhibited a marked linear relationship ($r^2 = 0.99$) (Fig. 1D). We conducted a second validation by comparing D of Dex4 with the corresponding D_{FRAP} , which exhibited a linear relationship ($r^2 = 0.9$) (Fig. 1E, illustrative FRAP measurements are shown in Suppl. Fig. S2). Third, we compared D and D_{FRAP} for all dextrans on dense COLI gels, and obtained a similarly good linear relationship ($r^2 = 0.99$, Suppl. Fig. S3). In average, the relative difference between D and corresponding D_{FRAP} data (Table 1) was $\sim 15\%$. Given the marked

technical and sample preparation differences between both techniques, the latter difference was deemed reasonable and D data were used in subsequent analysis.

3.2. Diffusion hindrance in ECM gels is consistent with the S-E equation

In all ECM gels, D decreased monotonically with M_r (Fig. 2A). Intriguingly, D of dense FIB was much larger than that of dense COLI and very close to rBM even though rBM was 3-fold denser than FIB. A decrease of D with M_r in free solution has been previously described in terms of power-laws ($D \sim M_r^{-\alpha}$) with a weak exponent $\alpha \sim 0.15-0.5$ [8, 14]. To check whether a similar description could be applied to our gel measurements, we fitted a power-law with a common exponent α simultaneously to all gels. The fittings exhibited a very good agreement with the experimental data ($r^2 = 0.99$) (Fig. 2A, continuous lines). Fitting parameters were $\alpha = 0.34 \pm 0.02$ (unitless), $D = (0.83 \pm 0.16) \times 10^{-5} M_r^{-\alpha}$ for rBM, $D = (0.99 \pm 0.18) \times 10^{-5} M_r^{-\alpha}$ for dense FIB, $D = (2.49 \pm 0.42) \times 10^{-5} M_r^{-\alpha}$ for dense COLI, and $D = (3.15 \pm 0.52) \times 10^{-5} M_r^{-\alpha}$ for sparse COLI, where the units of D and M_r are cm^2/s and Da, respectively. Notably, the fitted α matched the $1/3$ value predicted by the S-E relation in free solution as indicated in Eq. (6). A similar α was obtained in D_{FRAP} data from dense COLI gels (Suppl. Fig. S4). These findings reveal that, despite their entangled architecture, ECM gels behave as dilute solutions for particles with physiologic M_r in terms of diffusion.

3.3. Diffusivity analysis in terms of ECM viscosity

A major consequence of the validity of the S-E equation is that transport is regulated by viscous friction (Eq. (6)). To examine this possibility more closely, we used D data and Eq. (6) to assess the effective microscopic viscosity η . In agreement with the S-E relation, η values

obtained with different dextrans were very similar for all gels (Fig. 2B and Suppl. Table S1). The horizontal dashed line is the water viscosity (η_{water}) at 37°C, whereas the thick solid lines represent the average η for each gel. Maximum η values were obtained in rBM and dense FIB, and were ≥ 3.5 -fold larger than that of water. Conversely, η of sparse COLI was similar to η_{water} , whereas η of dense COLI was ~ 1.5 -fold larger than η_{water} . Of note, η of dense FIB were similar to rBM and ~ 3 -fold higher than dense COLI, highlighting that the viscosity of ECM gels (but not gel density) is predictive of the diffusion hindrance of dextrans with physiological M_r values.

3.4. Diffusivity analysis in terms of ECM geometry

A critical geometrical parameter of hydrogels in terms of diffusion is its average pore width (w), since geometrical effects are thought to be more relevant as the size of the particles approaches w [8, 12]. We used AFM imaging to assess w . All gels could be imaged except sparse COLI owing to its compliance. A representative image obtained in dense COLI is shown in Fig. 3A. Although ECM filaments were somewhat distorted during scanning, they remained stable enough to enable identifying pores as surface invaginations (Fig. 3A). Image analysis revealed a log-normal distribution of pore areas (Fig. 3B and Suppl. Fig. S5), which was used to calculate w (Fig. 3C). w from sparse COLI was included taking values reported elsewhere [28-31] for completeness' sake. We found a general reduction of w with gel density. However, unlike diffusivity, the w range for dense FIB was closer to that of dense COLI than to rBM. Our data also reveal that the median w were more than 100-fold larger than R_H of dextrans, even at the highest gel density.

3.5. Diffusion hindrance in ECM gels, cells and tissues

Tortuosity is commonly used to characterize diffusion hindrance in tissues and hydrogels, and is defined as $\lambda = (D_{free}/D_{medium})^{1/2}$, where D_{free} and D_{medium} are the diffusivity of the particle in free aqueous solution and in the specific medium, respectively [8, 10, 14]. According to the conformance of (D, M_r) data to the S-E equation, λ_{gel} could be assessed as $\lambda_{gel} = (\eta/\eta_{water})^{1/2}$, where η were taken as the average per gel (Fig. 3D). The results obtained revealed that $\lambda_{gel} \geq 1.3$ for all gel densities ≥ 3 mg/ml in all dextrans, whereas λ_{gel} values in sparse COLI (1 mg/ml) were comparable to 1, which is indicative of very weak hindrance as in free solution. As a guidance we plotted the average λ values attributable to cells only ($\langle \lambda_{cell} \rangle = 1.3$ (1.1-1.5)) [8-11] and those values measured with dextrans comparable to ours in brain tissue ($\langle \lambda_{brain} \rangle = 2.1$ (1.6-2.7), summarized in Table 2) [8, 14], which is considered among the most geometrically restrictive tissues in terms of diffusion. This comparison revealed that λ_{gel} measured in both rBM and dense FIB was in average 1.5-fold larger than $\langle \lambda_{cell} \rangle$, and that these λ_{gel} values fell within the same range than $\langle \lambda_{brain} \rangle$.

3.6. Convenient time-windows in 3D culture experiments based on diffusivity data

Diffusion sets a minimum time-window that must be contemplated to guarantee that all cells in a 3D culture are exposed to the same equilibrium concentration of the signaling factor. To assess a convenient time-window, we calculated the **time to reach half the equilibrium concentration** $t_{50\%}$ due to either λ_{gel} alone (dotted lines) or to gels and cells (λ_{3D}) as in 3D cultures (continuous lines) (Fig. 4). The latter tortuosity was assessed as $\lambda_{3D} \approx \lambda_{gel}\lambda_{cell}$ [8, 9, 32, 33], where λ_{cell} was taken as 1.3, eliciting $t_{50\%,ECM+cells} = 1.69t_{50\%,ECM}$, where $t_{50\%,ECM+cells}$ and $t_{50\%,ECM}$ are $t_{50\%}$ values in ECM gels in the presence of absence of cells, respectively. Plots of $t_{50\%}$ as a function of gel thickness for all conditions examined are shown in Fig. 4A-D. For ~ 2 mm

thick gels, $t_{50\%,ECM}$ was ~ 3 -4 days for the largest M_r in rBM and dense FIB, whereas it was < 1 day for COLI gels. These values almost doubled when considering the effect of λ_{cell} , indicating that considering λ_{gel} alone underestimates markedly the predicted t_{50} in 3D cultures.

4. Discussion

A simple and cost-effective method to assess the diffusivity of signaling molecules is desirable for cell biology groups working with 3D cultures. Our spectrophotometer-based assay—in which the intensity of fluorescently-labelled diffusing particles was analyzed within the diffusion layer—minimized the effects of photobleaching in the widely used FITC-dextran, and reported apparent diffusivity values that were $\sim 15\%$ lower in average than those obtained with FRAP. Comparing our D values with those reported elsewhere for similar dextrans and gels revealed a relative difference of $\leq 30\%$ for COLI gels and dense FIB [5, 34, 35]. We could not find previous D data for dextrans in rBM gels. Instead, the reported diffusivity of gold nanoparticles in rBM was $\sim 0.1 \times 10^{-6}$ cm²/s [34], which is very close to our D values at the highest R_H (Fig. 2A). Two major factors may account for the moderate discrepancy between our D and D_{FRAP} values. First, technical differences, since FRAP measured diffusivity of particles initially at equilibrium within a micrometer-sized region of the sample, whereas our spectrophotometer-based approach examined diffusion in bulk of particles towards equilibrium. Second, our theoretical modeling based on the computationally simple solution of Fick's law under the semi-infinite slab approximation, which was fitted within the diffusion layer. Moreover, our modeling assumed that: (1) the concentration above the gel was not decreased during the experiment, and (2) the diffusivity in the solution below the gel is the same as in the gel. The first assumption relies on the fact that we fitted Eq. (4) to the diffusion layer, i.e. far before the equilibrium

regime. In support of this assumption, a recent study conducted with a chemotaxis assay similar to ours on COLI gels reported a difference between diffusivity data obtained with the semi-infinite model applied within the diffusion layer or with Finite-Element (F-E) analysis of 17% [15], which is very close to the $\sim 15\%$ discrepancy between our D and D_{FRAP} values. The latter agreement suggests that the correction obtained with F-E analysis is modest, whereas it is much more computationally demanding. The second assumption is justified by the fact that the spectrophotometer measured the bulk fluorescence in the lower Transwell compartment, which is comparable to measuring right at the bottom of the gel ($x = l$). In addition to technical and theoretical limitations, the discrepancy between our D data and that reported elsewhere may be contributed by the different gel preparation and/or ECM source. Despite all these variability sources, it is remarkable the good agreement between our macroscopic diffusivity data and that obtained with FRAP and other microscopic assays. Accordingly, our work expands a recent study that used a Nanodrop spectrophotometer to assess the apparent diffusivity in scleral tissue [36], and altogether support that spectrophotometer-based assays provide a suitable and cost-effective alternative to assess the apparent diffusivity in ECM gels used in 3D cultures with reasonable accuracy.

Previous studies in tissues and non-ECM fibrous networks have attributed diffusion hindrance to either geometric (steric) or non-geometrical (viscous) effects of the network, or a combination of both [7, 10, 13, 37]. However, it had remained unclear what ECM effects dominate diffusion hindrance in conditions relevant for 3D cultures. Our AFM image analysis reported median ECM pore sizes $w \geq 0.4 \mu\text{m}$ for all gels (Fig. 3C), in agreement with previous studies using alternative imaging approaches [28-31, 38]. Since the maximum R_H was $\sim 5.5 \text{ nm}$, dextrans were 2 orders of magnitude smaller than the median w , indicating that they behaved as

small molecules in terms of diffusion. In these conditions we provided direct evidence that the relationship between the apparent D and M_r is well captured by the S-E equation (Fig. 2A). In further agreement with S-E, we observed a similar viscosity with each dextran for a given gel. These observations were not anticipated, since the S-E equation was derived for rigid spherical particles in a Newtonian liquid, which is in marked contrast with the entangled structure of ECM gels. In qualitative agreement with our findings, previous attempts to examine D dependence on M_r reported power-law relationships in both FIB and COLI gels [5, 9], although they could not unambiguously discriminate the $1/3$ power-law exponent from other possibilities. These results reveal that, at least for small particles, ECM gels at densities used in 3D cultures behave as dilute porous solutions. Moreover, these observations revealed that the enhanced ECM viscosity is the main physical gel property in controlling the transport of small spherical particles rather than ECM geometry.

We can envision two potential hydrodynamic effects underlying the enhanced ECM gel viscosity: (i) a wall effect due to the surface of the ECM scaffold, and (ii) the effect of unassembled ECM macromolecules. Wall-effects describe the flow reduction in the proximity of a 2D wall, which increases the effective viscosity of the fluid [39]. This wall-effect predicts that D should correlate with the median w . However, such prediction was not consistent with the similar D observed in rBM and dense FIB. Likewise, it could not account for the similar λ_{gel} measured in the latter ECM gels and those reported in the extracellular space (ECS) of brain tissue, whose pore sizes are much smaller than in ECM gels [8]. Alternatively, fluid viscosity is known to increase in the presence of soluble macromolecules [40, 41]. For dilute solutions, η increases linearly with the volume fraction occupied by the soluble large macromolecules ($\phi_{unattach}$). Although, to our knowledge, $\phi_{unattach}$ in an ECM gel remains unknown, we may assume

that it is linear with gel density d as a first approximation. In support of the latter prediction, we observed a fairly linear relation between η/η_{water} obtained in COLI and rBM gels and d (Fig. 5), which is reasonable considering the large content of collagen IV in rBM. The simplest model that relates η/η_{water} and $\phi_{unattach}$ for rod-like macromolecules like ECM filaments [29] is the Kuhn model [40, 41], which predicts $\eta/\eta_{water} = 1 + (5/2 + x)\phi_{unattach}$, where x is the axial ratio (length/width) of the rod. Taking a previously suggested value ($x = 19$) [41] elicited $\phi_{unattach} \sim 0.01$ (sparse COLI), ~ 0.04 (dense COLI), ~ 0.15 (rBM) and ~ 0.11 (dense FIB), which fell within the theoretical range of $\phi_{unattach}$ data assessed in brain tissue (0.18-0.5) [10]. Of note, the role of unassembled ECM molecules in enhanced viscosity is further substantiated by previous observations reporting undistinguishable dextran diffusivities obtained in dense COLI solutions before and after gelation [9] or in aligned and nonaligned sparse COLI gels [42]. All these observations strongly support that the enhanced ECS viscosity largely arises from unattached ECM macromolecules, and that the similar η in rBM and dense FIB is due to their comparable $\phi_{unattach}$. Moreover, these findings suggest that current models of diffusion hindrance in hydrogels should be revisited at least in ECM gels, since they do not consider the contribution of $\phi_{unattach}$.

Our results may improve the design of 3D culture studies in at least 3 directions. First, dense rather than sparse gels should be selected, since the latter fail to reproduce physiologic λ values even after adding the effect of λ_{cell} . Second, there is a minimum time-window that must be contemplated to guarantee that all cells in a 3D culture are exposed to the same equilibrium concentration of the signaling molecule for a given ECM gel. To assess such suitable time-windows, we used a simple model to predict t_{50} values. Noteworthy, our predictions were consistent with experimental time-windows reported in 3D culture studies (Table 3) [5, 18, 43, 44]. However, our predictions are likely to be an underestimation for soluble signaling

molecules, since many ECM components contain binding domains for signaling factors [7, 8]. Third, unwanted diffusion effects due to gel thickness can be minimized by using thinner gels according to Fig. 4. Thickness effects can be further reduced by preparing 3D cultures in Transwell inserts and adding the signaling factor both on top of the gel and in the bottom Transwell compartment. Alternatively, thickness effects may be simply prevented by culturing cells on top of the ECM gel instead of embedded when appropriate [3].

5. Conclusions

We provided a proof-of-principle that the spectrophotometers in commercial MultiPlate Readers and Transwell plates provide a simple and cost-effective alternative approach to assess the apparent diffusivity in ECM gels. Using this approach we found that the S-E relation derived for Newtonian fluids can be extended to the complex entangled structure of ECM gels. Accordingly, we clarified that the diffusion hindrance of small particles is regulated by the enhanced viscosity of the gel rather than by geometric factors, and provided a strong rationale that this enhanced viscosity is largely contributed by unassembled ECM macromolecules. In addition, we found that 3D cultures based on dense gels (≥ 3 mg/ml) were able to reproduce the large physiologic tortuosity of brain tissue and some tumors, underscoring that they are suitable tissue surrogates in terms of diffusion. Finally, we provided guidelines to improve the diffusive effects in 3D cultures.

Acknowledgements

We thank the Confocal Unit (CCiTUB), E. Rius (UB), F. Puig (Parc Taulí) and C. Ghajar (LBNL) for technical assistance, and I. Pagonabarraga (UB) for critical discussions. We also

thank A. Xaubet, N. Reguart (IDIBAPS), D. Navajas and R. Farré (UB) for support. This work was further supported by grants from the Ministerio de Economía y Competitividad (SAF2009-13243 and PI13/02368 to JA, CTM2012-39183-C02-02 to FM), Asociación Española Contra el Cáncer (to JA), Generalitat de Catalunya (2009SGR465 and XRQTC to FM), a Juan de la Cierva postdoctoral fellowship from Ministerio de Economía y Competitividad (To IP), and a pre-doctoral fellowship from the Ministerio de Educación (to AG).

Figure captions

Fig. 1. (A) Scheme of the experimental set-up. (B) Average fluorescence recorded with the Microplate Reader at different Dex4 concentrations. Continuous line indicates a linear regression fitting ($r^2 = 0.99$). (C) Fluorescence of Dex4 in the lower Transwell compartment measured with a Microplate Reader as a function of time in a panel of ECM gels. Fluorescence data were normalized to the maximum fluorescence measured in SFM. Continuous and dotted lines correspond to the fittings of the semi-infinite model up to either 50% of the last fluorescence data points or the entire data range, respectively, where the D was a fitting parameter ($n = 3$). D data obtained with the former fittings were used in the following sections. (D) Comparison between experimental D_{SFM} of all dextrans and the corresponding theoretical prediction D_0 assessed with the S-E equation. (E) Diffusivity data for Dex4 assessed in all samples with either the spectrophotometer-based assay or FRAP ($n = 6$).

Fig. 2. (A) D data as a function of M_r for each ECM gel. Continuous lines correspond to the simultaneous fitting of a power-law with a fixed exponent for all gels, being the exponent a fitting parameter. (B) Effective viscosity calculated using Eq. (6) and D data in (A). Dashed lines

correspond to the viscosity averaged for all M_r for each gel. Dashed horizontal line represents water viscosity at 37°C.

Fig. 3. (A) Representative topographic AFM image of the surface of a dense COLI gel in PBS. Scale bar corresponds to 5 μm . (B) Frequency distribution of pore areas outlined in the AFM images. (C) Log-scale box-plot of pore sizes calculated from AFM images ($n \geq 85$). Data of sparse COLI gels were reported elsewhere (see section 3.4 for details). *** $P < 0.005$ were determined by Mann-Whitney test. (D) λ_{gel} values calculated from η data shown in Fig. 2B. Horizontal lines indicate the average λ values reported from cells alone or in the extreme physiologic hindrance conditions of the brain tissue. * $P < 0.05$, ** $P < 0.01$ and *** $P < 0.005$ were determined by Student's t -test with respect to sparse COLI.

Fig. 4. Theoretical minimum experimental time-windows in 3D culture experiments as a function of gel thickness. $t_{50\%}$ values were assessed with Eq. (5) as $t_{50\%} = l^2 \lambda^2 / (1.69 D_o)$ using either λ_{gel} alone (dotted lines) or $\lambda_{3D} \approx \lambda_{gel} \lambda_{cell}$, taking $\lambda_{cell} = 1.3$ (continuous lines) for rBM (A), dense FIB (B), dense COLI (C) and sparse COLI (D). A different vertical scale between (A,B) and (C,D) was used for clarity purposes.

Fig. 5. Normalized viscosity with respect to water (Fig. 2B) as a function of gel density. Lines represent separate linear fittings of either all gels other than dense FIB (continuous) or dense FIB alone (dashed).

References

- [1] L.G. Griffith and M.A. Swartz. *Nat Rev Mol Cell Biol*, 7 (2006) 211-224.
- [2] A. Colom, R. Galgoczy, I. Almendros, A. Xaubet, R. Farré and J. Alcaraz. *J Biomed Mater Res A*, [Epub ahead of print] (2013).
- [3] J. Alcaraz, R. Xu, H. Mori, C.M. Nelson, R. Mroue, V.A. Spencer, D. Brownfield, D.C. Radisky, C. Bustamante and M.J. Bissell. *EMBO J*, 27 (2008) 2829-2838.
- [4] J. Alcaraz, H. Mori, C.M. Ghajar, D. Brownfield, R. Galgoczy and M.J. Bissell. *Integr Biol (Camb)*, 3 (2011) 1153-1166.
- [5] C.M. Ghajar, X. Chen, J.W. Harris, V. Suresh, C.C. Hughes, N.L. Jeon, A.J. Putnam and S.C. George. *Biophys J*, 94 (2008) 1930-1941.
- [6] H. Mori, A.T. Lo, J.L. Inman, J. Alcaraz, C.M. Ghajar, J.D. Mott, C.M. Nelson, C.S. Chen, H. Zhang, J.L. Bascom, M. Seiki and M.J. Bissell. *Development*, 140 (2013) 343-352.
- [7] M.A. Swartz and M.E. Fleury. *Annual Review of Biomedical Engineering*, Vol 9, Annual Reviews, Palo Alto, 2007, pp. 229-256.
- [8] E. Sykova and C. Nicholson. *Physiol. Rev.*, 88 (2008) 1277-1340.
- [9] S. Ramanujan, A. Pluen, T.D. McKee, E.B. Brown, Y. Boucher and R.K. Jain. *Biophys. J.*, 83 (2002) 1650-1660.
- [10] D.A. Rusakov and D.M. Kullmann. *Proceedings of the National Academy of Sciences of the United States of America*, 95 (1998) 8975-8980.
- [11] A. Shkilnyy, P. Proulx, J. Sharp, M. Lepage and P. Vermette. *Colloid Surf. B-Biointerfaces*, 93 (2012) 202-207.
- [12] A. Pluen, P.A. Netti, R.K. Jain and D.A. Berk. *Biophys. J.*, 77 (1999) 542-552.
- [13] R.J. Phillips. *Biophys. J.*, 79 (2000) 3350-3353.
- [14] R.G. Thorne, S. Hrabetova and C. Nicholson. *Journal of Neurophysiology*, 92 (2004) 3471-3481.
- [15] A. Vasaturo, S. Caserta, I. Russo, V. Preziosi, C. Ciacci and S. Guido. *PLoS One*, 7 (2012) 12.
- [16] P.V. Moghe, R.D. Nelson and R.T. Tranquillo. *J. Immunol. Methods*, 180 (1995) 193-211.
- [17] S. Raghavan, C.J. Shen, R.A. Desai, N.J. Sniadecki, C.M. Nelson and C.S. Chen. *J. Cell Sci.*, 123 (2010) 2877-2883.
- [18] J.E. Fata, H. Mori, A.J. Ewald, H. Zhang, E. Yao, Z. Werb and M.J. Bissell. *Dev Biol*, 306 (2007) 193-207.
- [19] J. Crank, *The mathematics of diffusion*, 2nd edition ed., Oxford University Press, Oxford, 1975.
- [20] A.J. Bard and L.R. Faulkner, *Electrochemical Methods. Fundamentals and Applications*, 2nd Ed. ed., Wiley, New York, 2001.
- [21] K. Braeckmans, L. Peeters, N.N. Sanders, S.C. De Smedt and J. Demeester. *Biophys. J.*, 85 (2003) 2240-2252.
- [22] T.K.L. Meyvis, S.C. De Smedt, P. Van Oostveldt and J. Demeester. *Pharm. Res.*, 16 (1999) 1153-1162.
- [23] I. Pastor, E. Vilaseca, S. Madurga, J.L. Garces, M. Cascante and F. Mas. *J. Phys. Chem. B*, 114 (2010) 4028-4034; *ibid*, 114 (2010) 12182
- [24] M.T. Sheu, J.C. Huang, G.C. Yeh and H.O. Ho. *Biomaterials*, 22 (2001) 1713-1719.

- [25] I. Horcas, R. Fernandez, J.M. Gomez-Rodriguez, J. Colchero, J. Gomez-Herrero and A.M. Baro. Review of Scientific Instruments, 78 (2007) 8.
- [26] M.D. Abramoff, P.J. Magelhaes and S.J. Ram. Biophotonics Int, 11 (2004) 36:42.
- [27] L. D.R., CRC Handbook of chemistry and physics, 89th edition ed., CRC Press. Taylor and Francis Group, LLC., 2008.
- [28] W. Mickel, S. Munster, L.M. Jawerth, D.A. Vader, D.A. Weitz, A.P. Sheppard, K. Mecke, B. Fabry and G.E. Schroder-Turk. Biophys J, 95 (2008) 6072-6080.
- [29] G.P. Raeber, M.P. Lutolf and J.A. Hubbell, Molecularly engineered PEG hydrogels: a novel model system for proteolytically mediated cell migration, Biophys J, 89 (2005) 1374-1388.
- [30] Y.A. Miroshnikova, D.M. Jorgens, L. Spirio, M. Auer, A.L. Sarang-Sieminski and V.M. Weaver. Phys Biol, 8 (2011) 026013.
- [31] M.H. Zaman, L.M. Trapani, A. Siemeski, D. Mackellar, H. Gong, R.D. Kamm, A. Wells, D.A. Lauffenburger and P. Matsudaira. Proc Natl Acad Sci U S A, 103 (2006) 10889-10894.
- [32] A. Pluen, Y. Boucher, S. Ramanujan, T.D. McKee, T. Gohongi, E. di Tomaso, E.B. Brown, Y. Izumi, R.B. Campbell, D.A. Berk and R.K. Jain. Proceedings of the National Academy of Sciences of the United States of America, 98 (2001) 4628-4633.
- [33] R.G. Thorne, A. Lakkaraju, E. Rodriguez-Boulan and C. Nicholson. Proceedings of the National Academy of Sciences of the United States of America, 105 (2008) 8416-8421.
- [34] B. Kim, G. Han, B.J. Toley, C.K. Kim, V.M. Rotello and N.S. Forbes. Nat. Nanotechnol., 5 (2010) 465-472.
- [35] T. Kihara, J. Ito and J. Miyake. Plos One, 8 (2013).
- [36] N. Srikantha, F. Mourad, K. Suhling, N. Elsaid, J. Levitt, P.H. Chung, S. Somavarapu and T.L. Jackson. Exp. Eye Res., 102 (2012) 85-92.
- [37] B.A. Westrin and A. Axelsson. Biotechnol. Bioeng., 38 (1991) 439-446.
- [38] Y.L. Yang, L.M. Leone and L.J. Kaufman. Biophys J, 97 (2009) 2051-2060.
- [39] J. Happel and H. Brenner, Low Reynolds number hydrodynamics: with special applications to particulate media, Dordrecht, The Netherlands, 1991.
- [40] M.L. Huggins. J. Phys. Chem., 42 (1938) 911-920.
- [41] R.R. Matheson. Macromolecules, 13 (1980) 643-648.
- [42] A. Erikson, H.N. Andersen, S.N. Naess, P. Sikorski and C.D. Davies. Biopolymers, 89 (2008) 135-143.
- [43] C.D. Roskelley, P.Y. Desprez and M.J. Bissell. Proc Natl Acad Sci U S A, 91 (1994) 12378-12382.
- [44] C.M. Nelson, M.M. Vanduijn, J.L. Inman, D.A. Fletcher and M.J. Bissell. Science, 314 (2006) 298-300.
- [45] M. Magzoub, S. Jin and A.S. Verkman, Faseb J., 22 (2008) 276-284.
- [46] L.J. Nugent and R.K. Jain, Cancer Res., 44 (1984) 238-244.
- [47] L.J. Nugent and R.K. Jain, Microvasc. Res., 28 (1984) 270-274.
- [48] P.A. Netti, D.A. Berk, M.A. Swartz, A.J. Grodzinsky and R.K. Jain, Cancer Res., 60 (2000) 2497-2503.
- [49] V.P. Chauhan, R.M. Lanning, B. Diop-Frimpong, W. Mok, E.B. Brown, T.P. Padera, Y. Boucher and R.K. Jain, Biophys. J., 97 (2009) 330-336.

- Diffusion hindrance in extracellular matrix (ECM) gels used in 3D cultures is investigated
- A cost-effective and simple spectrophotometer-based diffusivity assay is introduced, and complemented with FRAP and AFM measurements
- Diffusion hindrance is largely controlled by the enhanced ECM viscosity
- Unassembled ECM macromolecules may control ECM viscosity
- Dense (but not sparse) ECM gels are suitable tissue surrogates in terms of diffusion

Accepted Manuscript

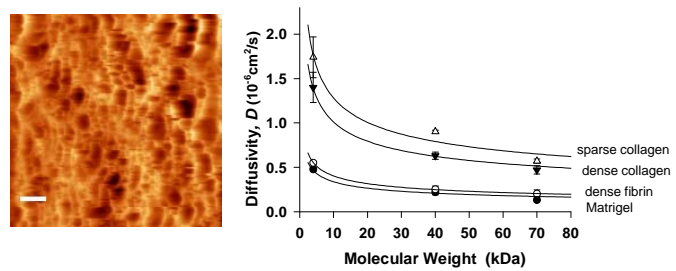


Figure 1

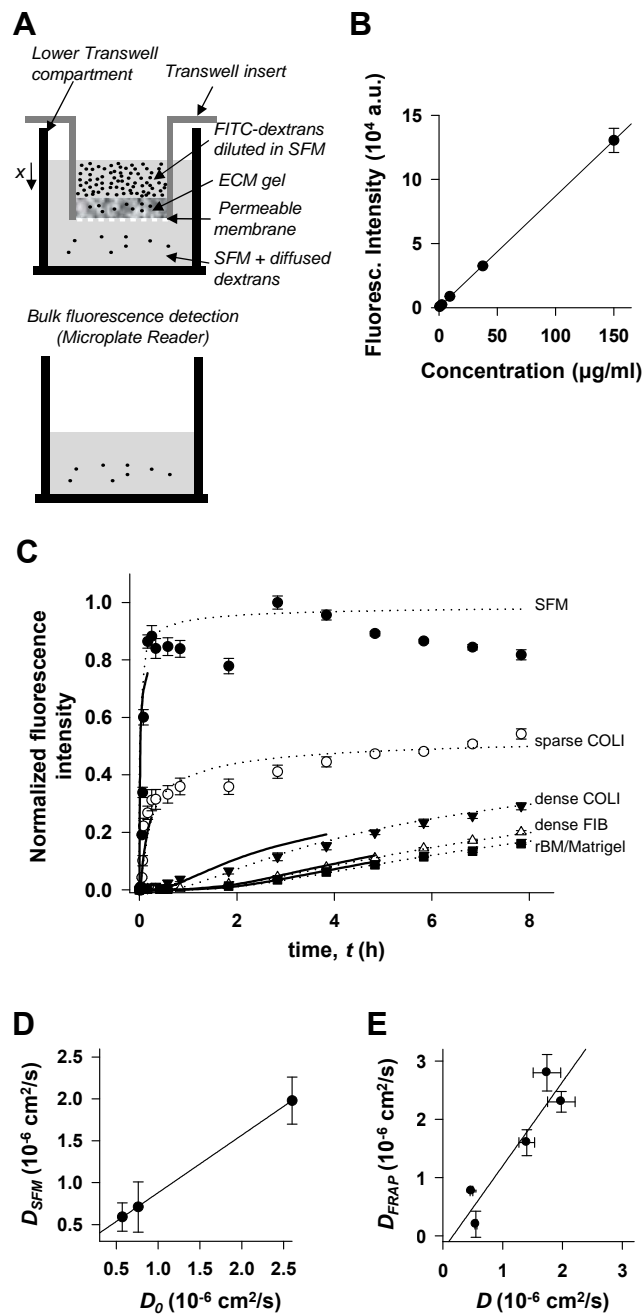


Figure 2

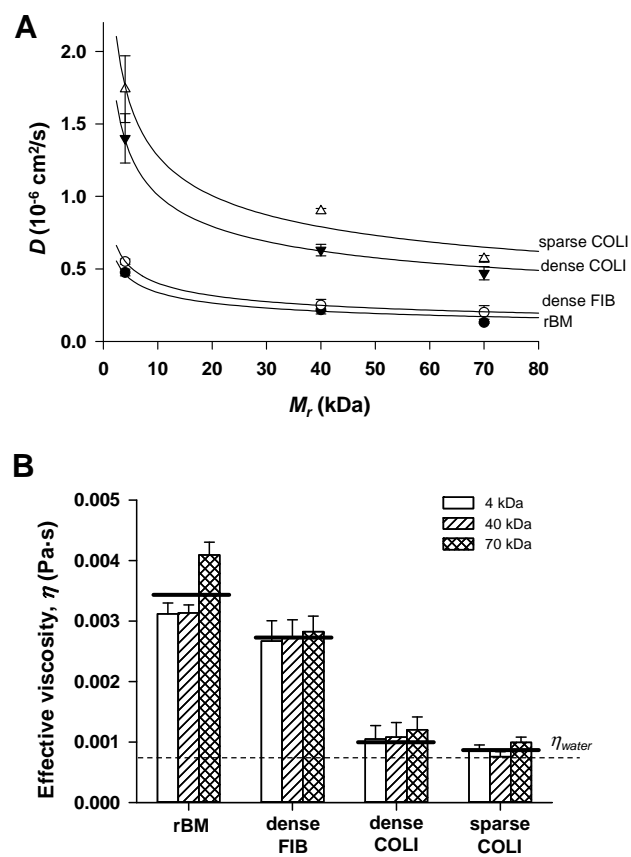


Figure 3

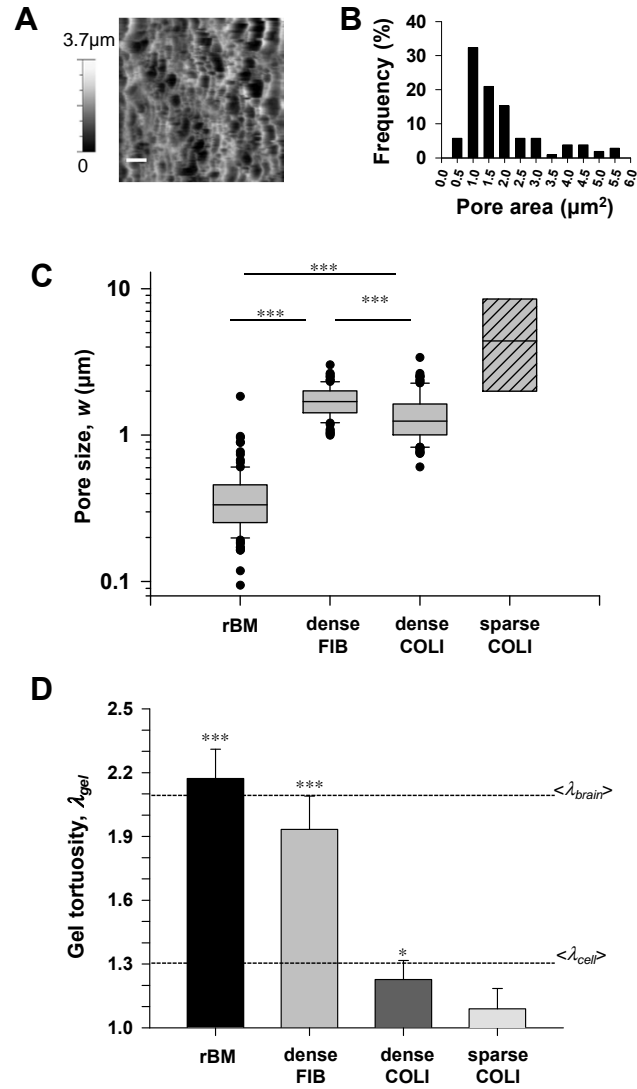


Figure 3

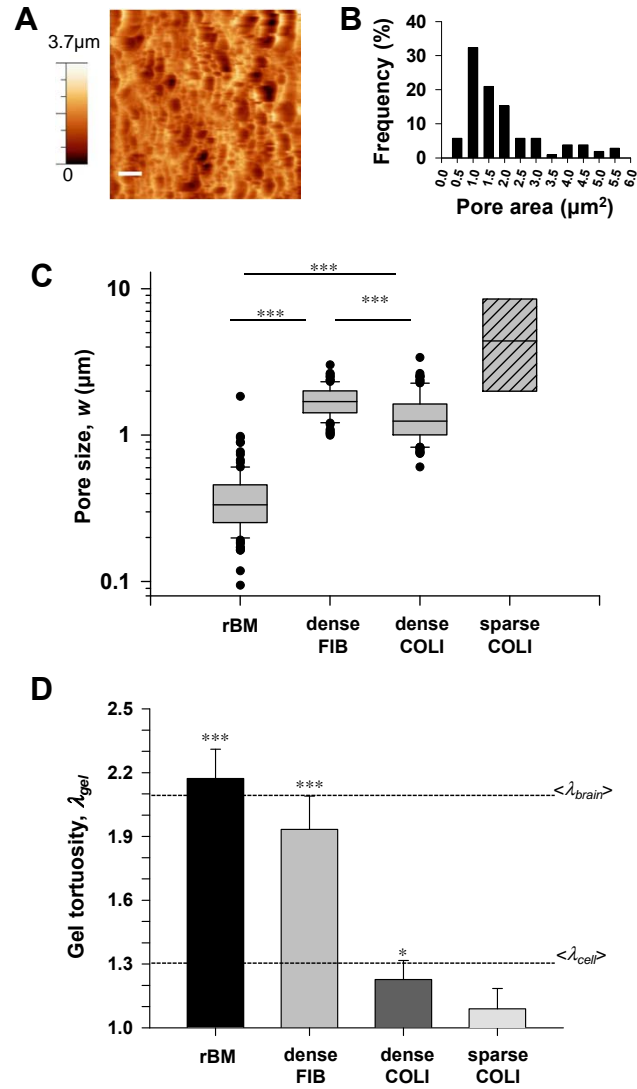


Figure 4

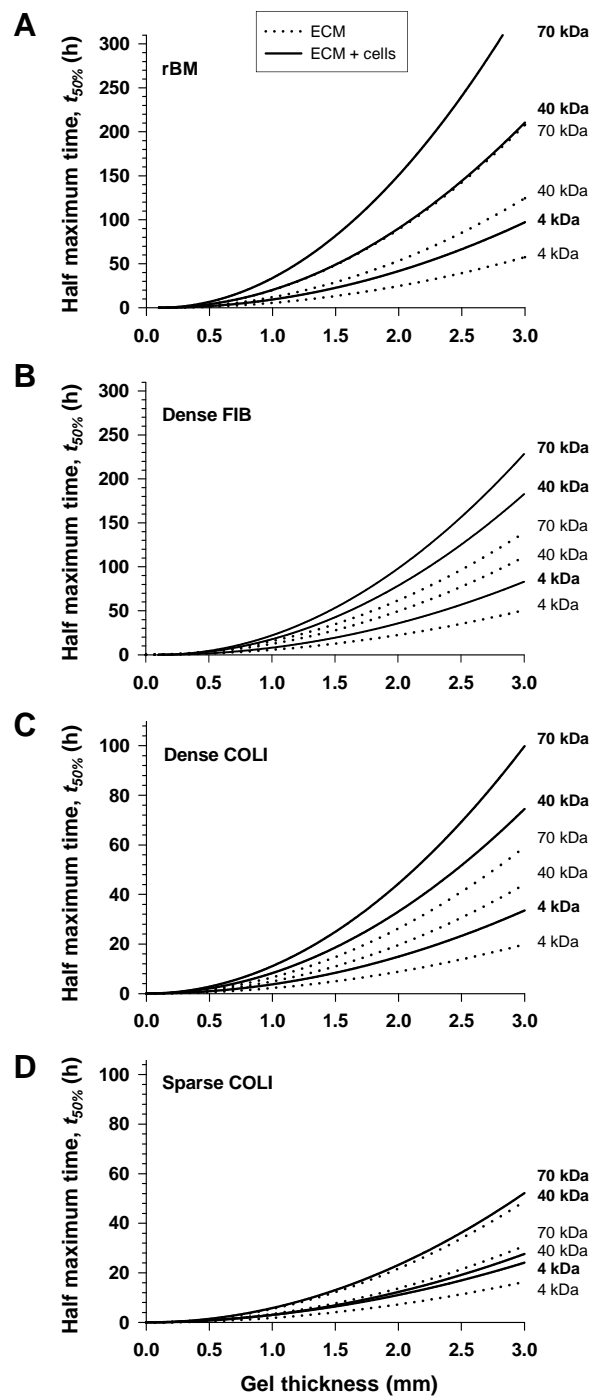


Figure 5

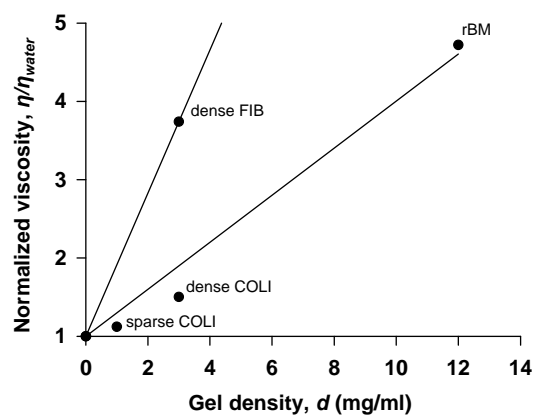


Table 1

Diffusivity values obtained with either S-E, the spectrophotometer-based assay within the diffusion layer, or FRAP (mean \pm SE)

Dextran M_r (kDa)	Sample	D (cm ² /s) (S-E)	D (cm ² /s) (diffusion layer)	D_{FRAP} (cm ² /s)
4kDa	rBM		$(4.7 \pm 0.2) \times 10^{-7}$	$(7.7 \pm 0.3) \times 10^{-7}$
	dense FIB		$(5.5 \pm 0.2) \times 10^{-7}$	$(3.7 \pm 0.6) \times 10^{-7}$
	dense COLI		$(14 \pm 2) \times 10^{-7}$	$(16 \pm 2) \times 10^{-7}$
	sparse COLI		$(17 \pm 3) \times 10^{-7}$	$(28 \pm 2) \times 10^{-7}$
	SFM	26×10^{-7}	$(19 \pm 3) \times 10^{-7}$	$(23 \pm 4) \times 10^{-7}$
40kDa	rBM		$(2.2 \pm 0.1) \times 10^{-7}$	n.a.
	dense FIB		$(2.5 \pm 0.1) \times 10^{-7}$	n.a.
	dense COLI		$(6.3 \pm 0.4) \times 10^{-7}$	$(7.9 \pm 0.2) \times 10^{-7}$
	sparse COLI		$(9 \pm 1) \times 10^{-7}$	n.a.
	SFM	7.6×10^{-7}	$(7 \pm 3) \times 10^{-7}$	n.a.
70kDa	rBM		$(1.3 \pm 0.1) \times 10^{-7}$	n.a.
	dense FIB		$(2.0 \pm 0.5) \times 10^{-7}$	n.a.
	dense COLI		$(4.7 \pm 0.6) \times 10^{-7}$	$(6.5 \pm 0.5) \times 10^{-7}$
	sparse COLI		$(5.7 \pm 0.8) \times 10^{-7}$	n.a.
	SFM	5.7×10^{-7}	$(5.9 \pm 1.7) \times 10^{-7}$	n.a.

Table 2 λ tissue values reported in the literature for dextrans and other macromolecules at different M_r

Tracer	Tissue	λ	Reference
EGF (6.6 kDa)	brain	1.8	[14]
Dex3	brain (cortex)	1.6-2	[8]
Dex3-Dex10	brain	1.8	[14]
Dex10	tumor xenograft	1.4-1.7	[45]
Different particle types ^I	normal granulation tissue	~1.1	[46]
Different particle types ^I	tumors xenograft	~1.15	[32]
Dex20	normal granulation tissue	2.3	[47]
Dex20	tumor implants	1.2	[47]
Dex40	brain (cortex)	2.16	[8]
Different particle types ^{II}	normal granulation tissue	~1.3	[46]
Dex40	tumors implants	1.3	[47]
Different particle types ^{II}	tumors xenograft	~1.5	[32]
Albumins ^{II}	tumors xenograft	1.6-2.8	[48]
Dex70	brain (cortex)	2.7	[8]
Dex40-70	brain	2.2	[14]
Albumins (14-66 kDa)	brain	2.1-2.5	[14]
Different particle types ^{III}	normal granulation tissue	~1.8	[46]
Dex70	tumors implants	1.8	[47]
Different particle types ^{III}	tumors xenograft	~1.9	[32]
Albumins ^{III}	tumors xenograft	1.6-2.6	[48]
IgG (150 kDa)	normal skin	1.4	[49]
IgG (150 kDa)	tumor xenograft	2.5	[49]

^Iat same R_H as Dex4; ^{II}at same R_H as Dex40; ^{III}at same R_H as Dex70

Table 3

Comparison between predicted t_{50} and experimental time-windows for selected 3D culture studies

Gel	Thickness	Signaling factor	predicted t_{50}	experimental time-window ^{II}	Reference
rBM	n.a.	Prolactin (22 kDa)	≥ 3 day ^I	3 day (β -casein expression)	[43]
rBM	~2 mm	TGF- α (17 kDa)	≥ 2.5 day ^I	2-3 day (robust branching)	[18]
dense COLI	n.a.	HGF (~80 kDa)	≥ 2 day ^I	1 day (early branching)	[44]
dense FIB	n.a.	vEGF, bFGF, HGF (~20-80 kDa)	~ 3-5 day ^I	7 day (robust branching)	[5]

^Ivalues based on a 2 mm gel thickness in Fig. 5; ^{II} t at which physiologic response was detected